

Bubble kinematics in a sheared foam

Yuhong Wang, Kapilanjani Krishan, and Michael Dennin

Department of Physics and Astronomy, University of California at Irvine, Irvine, California 92697-4575

(Dated: March 23, 2022)

We characterize the kinematics of bubbles in a sheared two-dimensional foam using statistical measures. We consider the distributions of both bubble velocities and displacements. The results are discussed in the context of the expected behavior for a thermal system and simulations of the bubble model. There is general agreement between the experiments and the simulation, but notable differences in the velocity distributions point to interesting elements of the sheared foam not captured by prevalent models.

PACS numbers:

I. INTRODUCTION

The microscopic kinematic response of a system to external forces can directly relate to its macroscopic properties. While the kinematic response of continuous media such as Newtonian fluids has been well characterized, theoretically as well as experimentally, understanding the behavior of non-Newtonian fluids and materials continues to be an area of active research [1, 2, 3, 4]. For both Newtonian and non-Newtonian fluids, the particle kinematics generally is characterized by velocity and position probability distributions [5, 6, 7, 8]. This is due to the large number of particles involved and the need for an inherently statistical description of the microscopic behavior. In studies of Newtonian fluids, the distributions are primarily governed by thermal fluctuations. In contrast, the fluctuations in many complex fluids are strongly coupled to the flow and structure of the constituent particles that are macroscopic objects, such as granular matter and bubbles, for which the relevant energy scales are significantly larger than thermal energies. This difference between thermal and athermal fluctuations can lead to qualitatively different explorations of phase space. It is therefore imperative to characterize not only the average flow behavior for complex fluids, but also the fluctuations of these particles.

The fluctuations in complex fluids are governed by the microscopic dynamics of the constituent elements of the fluid. The dynamics are influenced by the structure and interaction at these scales. Examples of such materials include cellular structures such as foams [9], fluids containing worm-like-micelles [10, 11] and large molecular mass solutions [12]. The constraints imposed by the structure influence the kinematic response (individual particle motions) at the microscopic scale [13]. In aqueous foams, the local structure consists of densely packed bubbles which elastically deform and rearrange their configuration in response to stresses. Such actuation occurs frequently, transitioning the system towards the various stable structural configurations accessible to the system. The rearrangements are strongly nonlinear and result in spatially and temporally localized changes in the velocity of the participating bubbles.

The kinematic response of various complex fluids has

been the subject of both experimental and theoretical work. For example, fluctuations of particles in granular matter have been heavily studied, especially in the context of kinematic models [6, 7, 14]. These fluctuations have important implications for the macroscopic rheology as they represent fundamental aspects of the flow at the microscopic scale.

Aqueous foams are ideal systems to investigate fluctuations [9]. As with granular matter, the structure has a sufficient influence on the dynamics that the length scale of interest is the size of the constituent bubbles rather than molecular dimensions. In contrast to granular matter, the primary constituent elements in such a material (air and water) are both Newtonian fluids. The dynamics are sufficiently overdamped that the system is effectively massless. This combination can lead to new behavior not observed in the granular systems and leads to interesting questions of the universality of the behavior that is observed in a range of complex fluids [8, 15].

Many past measurements of fluctuations in foam have focused on global quantities, such as stress fluctuations or fluctuations in energy. A number of simulations suggest various classes of interesting behavior for the fluctuations. Simulations for very dry foams, using a vertex model, propose power-law scaling for the stress fluctuations [16, 17]. Quasi-static simulations of wet foams that measured T1 events suggest power law scaling near the melting transition [18, 19]. (T1 events are events in which bubbles exchange neighbors.) In contrast, a q-potts model for foam only found evidence for power law scaling in distributions of energy fluctuations but not in the T1 event distributions [20].

Another interesting model is the bubble model [15, 21]. This treats a foam as a collection of spheres (or circles in two-dimensions) that experience two forces: (1) a spring force proportional to the overlap of bubbles and (2) a viscous drag force proportional to the velocity difference between two bubbles in contact. This model is most relevant for wet foams in which the bubbles are essentially spherical. Simulations of the bubble model suggest that power law scaling did not exist for energy fluctuations [15, 21, 22]. Instead, there is a well-defined average size of the stress fluctuations. Various experiments have used indirect measures of the fluctuations, and systems with

both power-law behavior [23] and a well-defined average [24, 25] have been reported. More recently, experiments using bubble rafts have directly measured the stress fluctuations and found behavior that is consistent with the predictions of the bubble model [26, 27]. (A bubble raft is a model two dimensional foam consisting of bubbles floating on a water surface [28].)

More recently, work has been carried out to characterize the statistics of the individual bubble motions. A significant study of velocity fluctuations and particle diffusion has been carried out for the bubble model [8]. One observes two distinct regimes of behavior as a function of the applied rate of strain. Below a critical rate of strain, a quasistatic regime is identified that is associated with a rate of strain independent average stress during flow. Above the critical rate of strain, the average stress increases with increasing rate of strain. A number of statistical measures exhibit different behavior above and below the critical rate of strain [8]. Given this relatively complete characterization of the bubble model, it is interesting to explore experiments that directly test these predictions. In this regard, the bubble raft is an ideal system as it models a wet foam in a manner that is very similar to the bubble model. By directly comparing the experiments and the model, one can gain insight into the usefulness of the approximations that are central to the bubble model. In this regard, some initial experiments with a bubble raft have tested the predicted scaling of the width of the velocity distribution. These experiments used a highly polydisperse system in a Couette geometry (flow between two concentric cylinders). The measurements of the width of the velocity distribution for this system agreed with similar prediction from the bubble model simulations [29].

In this paper we study the response of a bubble raft when subjected to parallel shear. When sheared, the velocity profile of the bubbles forming the foam are seen to asymptotically converge to that of a Newtonian fluid. However, the fluctuations in the velocity profiles are seen to play an important role in describing the impact of the inherent coarse cellular structure of the foam. The rest of the paper is organized as follows. Section II describes the experimental methods. Section III presents the results, and Sec. IV provides a discussion of the results in the context of both the simulations results in Ref. [8] and the earlier experiments reported in Ref. [15]. Section IV also discusses interesting directions for future work.

II. EXPERIMENTAL METHODS

Our experiments characterize the motion of individual bubbles of a bubble raft when subjected to shear. The bubble raft is produced by flowing regulated nitrogen gas through a needle into a homogeneous solution of 80% by volume deionized water, 15% by volume glycerine, and 5% by volume Miracle Bubbles (from Imperial Toy Corporation). The bubble size is dependent on the flow

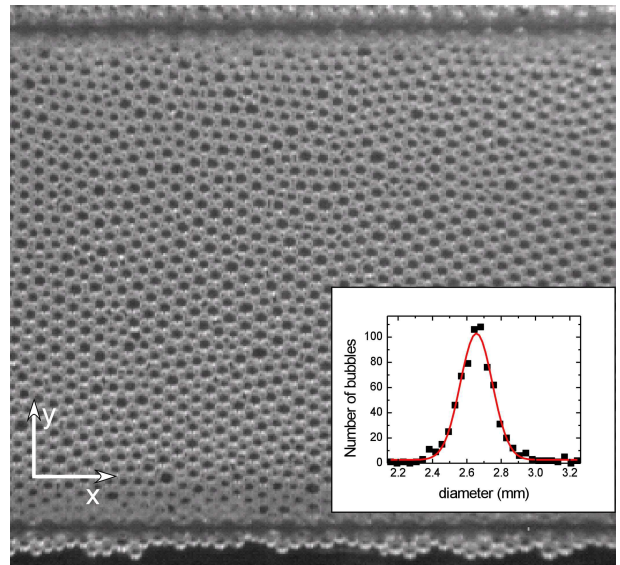


FIG. 1: A typical image representing the instantaneous structure of the bubble raft. Shear induced through the bands on the top and bottom cause the material to yield through slip between neighboring bubbles (T1 events). These local events cause fluctuations in the velocity profiles of the bubbles, that average out over long times. Insert is a typical distribution for the bubble sizes.

rate of the nitrogen gas as well as the depth of the needle in the water layer. This system forms a two-dimensional wet foam on a homogeneous liquid substrate. The bubble raft formed consists of a tightly packed configuration of bubbles as seen in Fig. 1. We use relatively monodisperse bubbles in our experiments because they are reproducible and easy to control. The typical mean bubble diameter is 2.66 mm. A typical size distribution is shown in the insert to Fig. 1. The width of the distribution is of the order 0.2 mm. The bubble raft is sheared by two parallel and counter-rotating bands driven by a stepper motor. The x-direction (\hat{i}) is taken parallel to the direction of motion of the bands, and the y-direction (\hat{j}) is taken perpendicular to the direction of motion of the bands, as indicated in Fig. 1.

The motion of bubbles are recorded using a CCD camera. The frame rate of the CCD camera is kept high enough so as to enable identifying individual bubbles between successive images. The digitized images are analyzed to yield the positions and velocities of individual bubbles during shear. The experimental setup has been previously discussed in detail in [30].

During each run, the bubbles are subjected to a total macroscopic shear strain of $\gamma \equiv \Delta x/D = 5$, where Δx is the total displacement the band and $D = 57$ mm is the distance between the two bands. This permits us to carry out our experiments in a reasonable time frame constrained by the life-time of the bubbles forming the raft when the shear rate is low. We find this amount of strain suffices in investigating the asymptotic behavior

of the system [30]. The velocity of the driving bands is $v_w \hat{\mathbf{j}}$, and the rate of strain is given by $\dot{\gamma} = 2v_w/D$. In this setup, the limits for the rate of strain are 10^{-3} s^{-1} to 10^{-1} s^{-1} .

The image analysis techniques to measure the positions of the bubbles are also detailed in [30]. The central one-third of the trough are used for all measurements reported in this paper. This region is found not to be strongly influenced by the entry-effects at the ends of the flowing zone. The instantaneous (for experimental purposes) velocity of a bubble is computed by considering the distance travelled by an individual bubble between successive frames recorded by the CCD camera. A longer time average may also be computed by considering the displacement of the bubbles between images recorded over the appropriately selected longer time. When discussing spatial dependence of the various measures, we spatially divide the bubble raft into equally spaced bins with a width of 1.4 mm in the y-direction. The bins are rectangular in shape as they extend over the middle third of the system in the x-direction.

In this paper we are primarily interested in detailing the probability distribution for the velocity and the nature of the bubble displacements. In order to characterize these quantities, we report on a number of different measures. First, we consider the root mean squared deviation of the velocity from its average value. This is done separately for the x- and y-component, and it is given by $\delta v_i = \sqrt{\langle (v_i(y) - \bar{v}_i(y))^2 \rangle}$. In this expression, i indicates the x or y-component of the velocity and $v_i(y)$ refers to the instantaneous velocity component of a bubble. $\bar{v}_i(y)$ denotes the average of these velocities in a given bin (indicated by the y-position of the bin) over the total strain applied. The braces, $\langle \rangle$, refer to an average over all bubbles being considered. This provides a measure of the width of the velocity distribution. We also consider the full probability distribution for the velocity, usually for an individual bin in the y-direction. For comparison with results using the bubble model, we also consider the probability distribution for the deviation of the velocity from a linear profile $\Delta \mathbf{v} \equiv \mathbf{v} - \mathbf{v}_L$ where \mathbf{v}_L is a linear profile defined by $\mathbf{v}_L(x) \equiv 2v_w(x/D)\hat{\mathbf{j}}$. Here $-D/2 \leq x \leq D/2$, where L is the distance between the driving bands. Finally, we characterize the bubble displacements by consider the mean square displacement of the bubbles as a function of time ($\langle (\Delta x)^2 \rangle$).

III. RESULTS

The most basic characterization of the fluctuations is given by the velocity probability distribution. We first consider the probability distributions for different spatial bins. The results for the center bin are presented in Fig. 2 for both the x-component (Fig. 2a) and y-component (Fig. 2b) of the velocity. As one expects, the distributions are centered at zero for the center bins, as the average velocity profile goes through zero in the

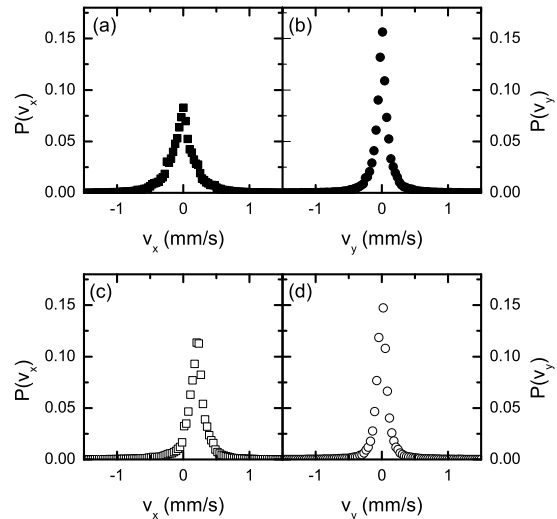


FIG. 2: (a) Probability distribution for v_x for bubbles in the central bin of the system. (b) Probability distribution for v_y for bubbles in the central bin of the system. (c) Probability distribution for v_x for bubbles in the bin half way between the center and the edge of the system. (b) Probability distribution for v_y for bubbles halfway between the center and the edge of the system. All plots correspond to a shear rate of 0.0056 s^{-1} .

center of the system. Both distributions are symmetric and are well-fit by a Lorentzian function.

Slightly different behavior is observed when considering the distribution of velocities in an off-center bin. In this case, one observes no fundamental change in the distribution of the y-component (Fig. 2d). The average v_y is expected to be zero throughout the system, and this is consistent with the observed symmetric distribution centered at $v_y = 0$. However, the distribution for v_x is asymmetric. One measure of the asymmetry is the third moment of the distributions. For comparison, the distributions in Fig. 2a-d have third moments of 6.4×10^{-5} , 4.9×10^{-4} , -1.4×10^{-2} , and 7.1×10^{-5} , respectively. Therefore, the measured asymmetry for the off-center v_x distribution is two to three orders of magnitude larger than any of the other distributions. This has the interesting consequence that the most probable value for v_x is different from the average value.

For a thermal distribution of velocities, such as one might find in an ideal gas, the width of the velocity distribution is related to the temperature through the distribution for kinetic energy. For the bubble raft, the system is highly overdamped and the bubbles are effectively massless. Therefore, it is not clear how one connects the velocity distribution with a temperature. Nonetheless, various proposals exist for defining an effective temperature as a function of the applied rate of strain, therefore, it is useful to consider the rate of strain dependence of the width of the velocity distribution. For direct com-

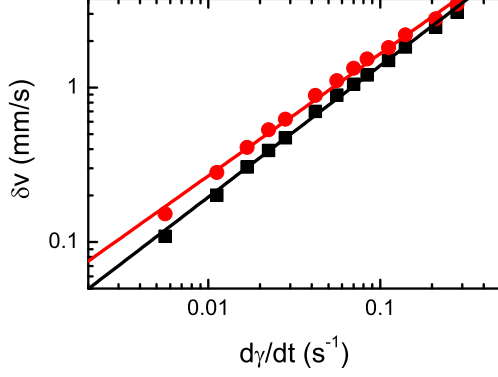


FIG. 3: (color online) The spread of the velocity distributions is seen to increase with increasing strain rate as a power law. The red circles (x-component) and black squares (y-component) refer to the width of velocity fluctuations in a central bin of the sheared bubbles. The solid lines are fits to the corresponding data.

parison of the results of Ref. [8] and [29], we characterize the width of the distributions using δv_i for the central bins. This choice avoids complications due to asymmetry at bins near the edges. Both δv_x and δv_y increase with increasing rate of strain. For the range of rates of strain studied here, the dependence is consistent with a power law with an exponent of 0.85 ± 0.01 for δv_y (circles in Figure 3) and 0.79 ± 0.02 (squares in Figure 3) for δv_x .

Following the characterization of the fluctuations in Ref. [8], we also consider the probability distributions for Δv_x and Δv_y . This distribution is computed over all position bins. The behavior of Δv_y is consistent with the expected behavior based on other characterizations (see Fig. 4). The width of the distribution increases with increasing rate of strain, reflecting the increased flux of energy into the system being distributed.

The behavior for Δv_x indicates interesting departures from previous studies. Again, the width of the distribution increases with increasing rate of strain. However, there is a well-defined peak in the distribution for slow rates of strain. As indicated in Fig. 5a, the peak decreases in amplitude as the rate of strain increase, and eventually disappears for rates of strain greater than 0.1 s^{-1} . The peak is highly asymmetric, demarcating a sharp decline in probability for larger velocity fluctuations from a gradual drop at lower ones. The value of the peak as a function of rate of strain is plotted in Fig. 6. The scaling of this should be compared with the width of the velocity distributions in Fig. 3. In contrast to the behavior of the distribution widths, the location of the peak is consistent with a linear dependence on rate of strain. This scaling is illustrated in Fig. 5b where we scale the x-axis by the rate of strain. We observe a number of features of the distribution by doing this. First, as expected, the loca-

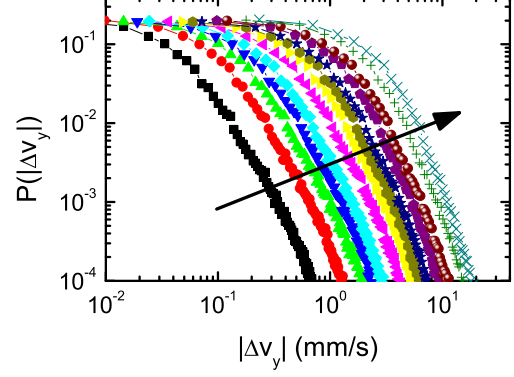


FIG. 4: (color online) Distribution of fluctuations in velocity along the y-direction for all bubbles. The different symbols (colors) represent different rates of strain, with the arrow indicating the direction of increasing strain.

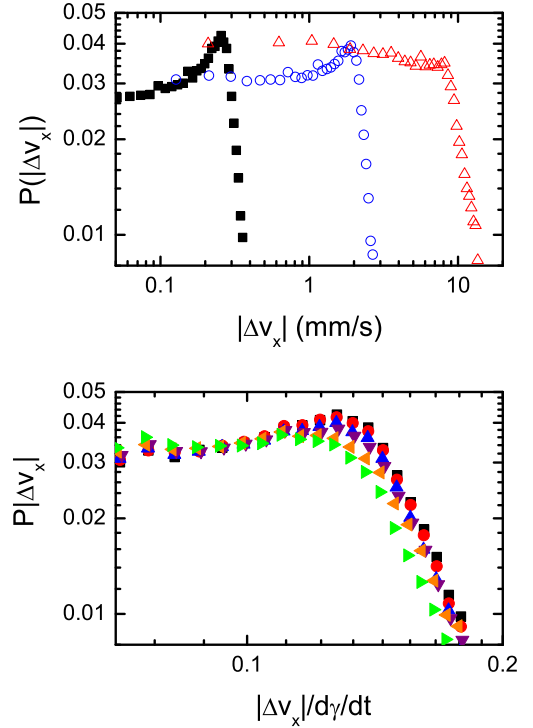


FIG. 5: (color online) (a) Probability distribution of fluctuations in velocity along the x-direction (Δv_x) for all bubbles for rates of strain of 0.0056 s^{-1} (\blacksquare), 0.042 s^{-1} (blue \circ), 0.21 s^{-1} (red \triangle). The three curves illustrate the existence of peak that disappears at higher rates of strain. (b) Probability distribution of fluctuations in velocity along the x-direction (Δv_x) for all bubbles for a range of rates of strain. Here Δv_x is scaled by the rate of strain. This highlights the linear dependence of the peak on the rate of strain.

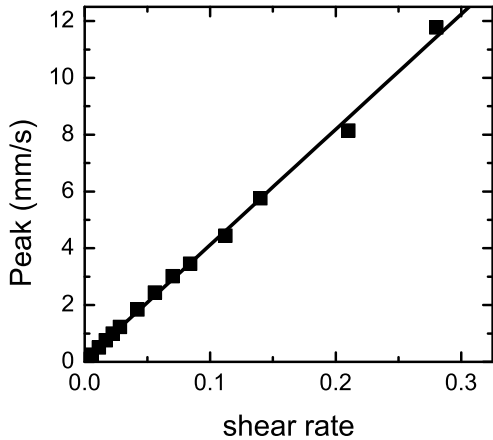


FIG. 6: Location of the peak in the distribution of velocity fluctuations in the x-direction as a function of rate of strain (symbols). The line is a linear fit.

tion of the peaks coincide, but the amplitude of the peak is clearly decreasing. Second, some variation is noted in the tail of the distributions, indicating that the distributions do not scale perfectly with rate of strain. This may be attributed to the power-law scaling of the width of the velocity distributions.

We tested the robustness of the peak by determining this distribution for a number of runs at the same rate of strain but with different configurations of bubbles. Though there was some variation in the amplitude of the peak from run to run, the peak was a distinct feature in each run.

Velocity distributions are not directly informative on the dynamics of individual bubbles. The second set of measures focuses on the particle displacements. For the data presented here, we focus exclusively on the motion in the y-direction and on bubbles that start in the central bin. This is done to discriminate transport induced due to the underlying constant shear along the x-direction. The motion of these bubbles is approximately diffusive. One measure of this is to compute the histogram of displacements for a given starting position for a bubble. This is shown as a function of time for a rate of strain of 0.0056 s^{-1} in Fig. 7. We observe the width of the distribution to be increasing in time, consistent with a diffusive process.

Another way to characterize this motion is to consider directly the mean square displacement of the bubbles as a function of time ($\langle (\Delta x(t))^2 \rangle$). This is shown in Fig. 8 for bubbles starting from three different locations in the trough: the central bin and two bins chosen symmetrically on either side of the central bin. As expected for diffusion, the behavior of $\langle (\Delta x(t))^2 \rangle$ is essentially linear in time in the central bin. For the off center bins, the

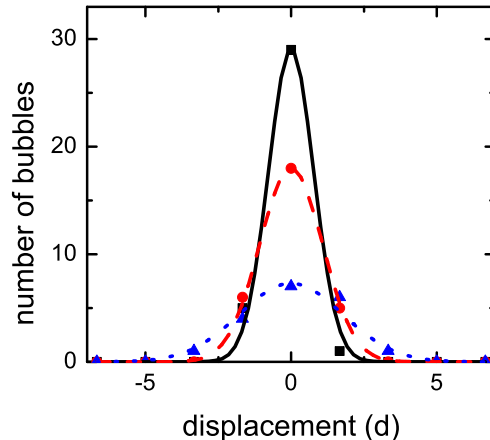


FIG. 7: (color online) Plotted here are the number of bubbles that start in the central bin that experience a particular displacement (in units of the bubble diameter d) in a given time. The symbols are the data for three different times: 25 s (■), 100 s (red ●), and 320 s (blue ▲). The curves are fits of each set of data to a Gaussian distribution.

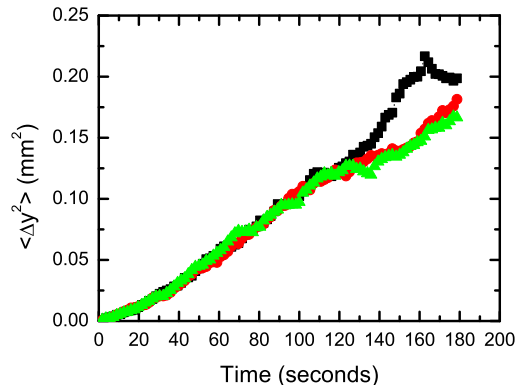


FIG. 8: (color online) Plotted here is $\langle (\Delta x(t))^2 \rangle$ averaged over all the bubbles as a function of time starting in three different initial bins: the central bin (■), 8.55 mm from one band (red ●), and 8.55 mm from the other band (green ▲). For the off center locations, we observe the expected symmetric behavior, with some deviation from linear at late times due to the influence of the boundaries.

displacements at longer times are suppressed. This is presumably due to the confining effects from the boundaries of the flow region.

An interesting feature of the data is the fact that for extremely short times (less than 15 seconds) the behavior clearly deviates from linear. In a system of particles in a gas, one would expect this for time scales short enough

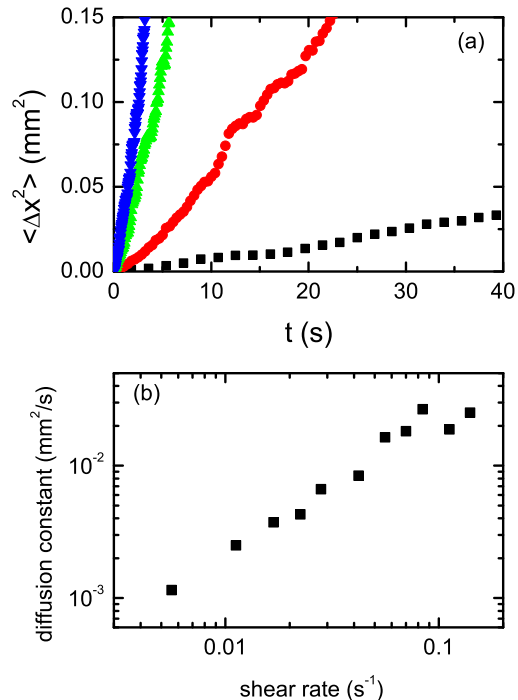


FIG. 9: (color online) (a) The $\langle (\Delta x(t))^2 \rangle$ averaged over all the bubbles as a function of time for bubbles from the central bin at four different rates of strain: 0.0028 s^{-1} (■); 0.014 s^{-1} (red ●); 0.07 s^{-1} (green ▲); and 0.14 s^{-1} (blue ▼). (b) Diffusion constants for motion transverse to the direction of flow as a function of rate of strain. The diffusion constants are based on the behavior of bubbles in the central bin, and they are seen to scale as a power-law with the rate of strain.

that ballistic motion is observed. For the bubbles, these short times presumably correspond to the linear motion of bubbles in between the T1 events and corresponding bubble rearrangements. We are currently pursuing more detailed tracking of individual bubbles to determine the exact nature of the short time behavior.

As a first approximation, we characterize $\langle (\Delta x(t))^2 \rangle$ as growing linearly with time. We can use this to estimate the effective diffusion constant for individual bubbles along the y-direction. Figure 9a is a plot of $\langle (\Delta x(t))^2 \rangle$ for a range of rates of strain for bubbles in the central bin. The slope of these curves yield the diffusion constant, and this is plotted in Fig. 9b. Unfortunately, the range of rate of strain that we were able to access is relatively small in comparison to numerical simulations as in [8]. In this limited range, the diffusion constant shows a linear dependence on the rate of strain.

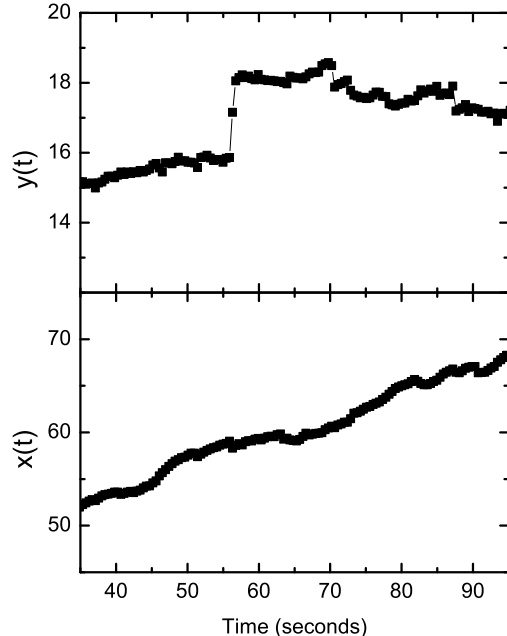


FIG. 10: The above plots indicate the x- and y-displacements of a single bubble with time. The fluctuations are qualitatively different, with ballistic-like transport dominating the shear direction and motion similar to Levi-flights in the transverse direction.

IV. DISCUSSION

We have performed an extensive investigation of kinematics associated with a sheared bubble raft. A striking feature of the results is the nature of the probability distributions of the velocity. For the distributions in the central region of the trough, they are well-fit by Lorentzian functions. This is very different from what one would expect for a thermal distribution of velocities. At this point, more work is needed on the individual bubble kinematics to determine the source of this distribution. But, a potential candidate is the highly overdamped dynamics.

The other feature of the distributions that requires further study is the asymmetry that develops in the probability distribution for v_x when bubbles that are off-center are considered. One potential explanation is the influence of the boundaries. However, there does not appear to be any similar asymmetry in the distribution for v_y . This suggests that the boundaries are not the source of the asymmetry, as one might expect the boundaries to influence both v_x and v_y . A related issue is the slightly nonlinear behavior of the average value of v_x . The source of the nonlinearity and the asymmetry of the probability distribution may be connected. Further work will be done in this area.

When summarizing the results of these experiments, it is especially helpful to compare and contrast them with

numerical studies of the bubble model that have guided earlier investigations. Not surprisingly, the general qualitative behavior matches the bubble model. A key element of the bubble model is the existence of a critical rate of strain [8] that is identified by a changes in the behavior of various quantities. One quantity in particular is the probability distribution of v_y . In the bubble model, this distribution develops a significant flat region for small values of v_y above a critical rate. We did not observe this behavior, and the measured distributions of v_y all suggest that the rate of strains studied in this paper are below the critical rate of strain.

Another measurement for which we observed reasonable qualitative agreement between the experiment and the bubble model simulations is in regard to the diffusion constant. However, we are unable to make a number of quantitative comparisons. First, it would be useful to study a wider range of rates of strain, particularly higher ones. However, currently we are limited in our studies of diffusion at higher rates of strain due to bubble lifetimes and the fact that they are eventually swept out of the system. Similar issues prevented calculating the diffusion constant from velocity correlation functions. These measurements will require either a longer system or the use of a Couette geometry which mimics periodic boundary conditions.

Despite the generally good qualitative agreement, there are some disagreements between our measurements and the bubble model. For example, the exponent for the power-law scaling of the width of distribution for velocity fluctuations is different for the bubble model studies reported in Ref. [8] and this current work. However, it should be noted that other work on fluctuations in a Couette geometry [29] were consistent with the work of Ref. [8]. When comparing the current work to Ref. [29], there are two main differences: geometry and degree of polydispersity. As the geometry is the same between this work and the simulations of the bubble model, it is most likely that the exact value of the exponent for the scaling of fluctuations is sensitive to the polydispersity. Future work will be able to test this systematically.

A more significant departure from results in the bubble model [8] and our measurements is the existence of a peak in the Δv_x distribution. More experimental work is needed to determine the source of this peak. Two obvious

candidates are the the asymmetry of the velocity distributions or a characteristic associated with the details of the bubble rearrangements. As the asymmetry in the velocity distribution near the boundaries is unique to our experimental study, this is definitely an effect that is not captured by the bubble model and could explain the lack of a peak in the velocity distribution. However, it is also possible that the details of the bubble rearrangements differ between the bubble rafts and the bubble model. This is one motivation for a closer look at individual bubble kinematics in the experiments.

One element missing from the bubble model is the attractions between the bubbles. This is an obvious candidate as the source of the quantitative disagreements between the bubble model simulations and our experiments. Incorporating such attractive effects in numerical models may help remove discrepancies with experiments.

For a number of the open questions, we have commented on the need for more detailed studies of the individual bubble dynamics. As useful as the collective studies reported in this paper, studies of individual particle kinematics provide insights into mechanisms of the microscopic transport taking place. Figure 10 illustrates the type of behavior that requires further study. In Fig. 10, we note the different qualitative behavior in transport transverse and longitudinal to the shear for a single bubble. There is an almost linear dependence of displacement with time along the x-direction due to the imposed flow. In the y-direction, the bubbles experience periods of extremely small displacements punctuated with large fluctuations. These fluctuations are of the length scale of about a bubble diameter, and may be attributed to the occurrence of T1 events in the immediate neighborhood of the bubble. It will be interesting to connect this behavior to similar motions in glassy systems [31, 32], and we are currently developing measures characterizing this qualitatively different transport.

Acknowledgments

This work was supported by a Department of Energy grant DE-FG02-03ED46071.

-
- [1] L. D. Landau and E. M. Lifshitz, *Fluid Mechanics, Second Edition : Volume 6 (Course of Theoretical Physics)* (Butterworth-Heinemann, 1987).
 - [2] J. P. Boon and S. Yip, *Molecular Hydrodynamics* (Courier Dover Publications, 1992).
 - [3] S. Chandrasekhar, *Hydrodynamic and Hydromagnetic Stability* (Courier Dover Publications, 1981).
 - [4] G. K. Batchelor, *An Introduction to Fluid Dynamics* (Cambridge University Press, 2000).
 - [5] M. Moseler and U. Landman, *Science* **289**, 1165 (2000).
 - [6] N. Mennon and D. J. Durian, *Science* **275**, 1920 (1997).
 - [7] W. Losert, D. G. W. Cooper, J. delour, A. Kudrolli, and J. P. Gollub, *Korea-Australia Rheology Journal* **9**, 682 (1999).
 - [8] N. Mennon and D. J. Durian, *Phys. Rev. E* **67**, 021405 (2003).
 - [9] D. Weaire and S. Hutzler, *The Physics of Foams* (Clarendon Press, Oxford, 1999).
 - [10] B. Chakrabarti, M. Das, C. Dasgupta, S. Ramaswamy, and A. K. Sood, *Phys. Rev. Lett.* **92**, 055501 (2004).

- [11] R. Ganapathy and A. K. Sood, Phys. Rev. Lett. **96**, 108301 (2006).
- [12] G. H. McKinley, O. Brauner, and M. Yao, Korea-Australia Rheology Journal **13**, 29 (2001).
- [13] M. Dennin, Phys. Rev. E **70**, 041406 (2004).
- [14] D. M. Mueth, Phys. Rev. E **67**, 011304 (2003).
- [15] D. J. Durian, Phys. Rev. Lett. **75**, 4780 (1995).
- [16] K. Kawasaki, T. Nagai, and K. Nakashima, Phil. Mag. B **60**, 399 (1989).
- [17] T. Okuzono and K. Kawasaki, Phys. Rev. E **51**, 1246 (1995).
- [18] D. Weaire, F. Bolton, T. Herdtle, and H. Aref, Phil. Mag. Lett. **66**, 293 (1992).
- [19] S. Hutzler, D. Weaire, and F. Bolton, Phil. Mag. B **71**, 277 (1995).
- [20] Y. Jiang, P. J. Swart, A. Saxena, M. Asipauskas, and J. A. Glazier, Phys. Rev. E **59**, 5819 (1999).
- [21] D. J. Durian, Phys. Rev. E **55**, 1739 (1997).
- [22] S. Tewari, D. Schiemann, D. J. Durian, C. M. Knobler, S. A. Langer, and A. J. Liu, Phys. Rev. E **60**, 4385 (1999).
- [23] A. A. Kader and J. C. Earnshaw, Phys. Rev. Lett. **82**, 2610 (1999).
- [24] A. D. Gopal and D. J. Durian, Phys. Rev. Lett. **75**, 2610 (1995).
- [25] M. Dennin and C. M. Knobler, Phys. Rev. Lett. **78**, 2485 (1997).
- [26] J. Lauridsen, M. Twardos, and M. Dennin, Phys. Rev. Lett. **89**, 098303 (2002).
- [27] E. Pratt and M. Dennin, Phys. Rev. E **67**, 051402 (2003).
- [28] L. Bragg and W. M. Lomer, Proc. R. Soc. London, Ser. A **196**, 171 (1949).
- [29] M. Dennin, Colloids and Surfaces, A: Physiochem. and Eng. Asp. **263**, 76 (2005).
- [30] Y. Wang, K. Krishan, and M. Dennin, Phys. Rev. E **73**, 031401 (2006).
- [31] E. R. Weeks and D. A. Weitz, Phys. Rev. Lett. **89**, 095704 (2002).
- [32] C. Donati, J. F. Douglas, W. Kob, S. J. Plimpton, P. H. Poole, and S. C. Glotzer, Phys. Rev. Lett. **80**, 2338 (1998).